Eur. Phys. J. C (2023) 83:749
https://doi.org/10.1140/epjc/s10052-023-11740-3

THE EUROPEAN PHYSICAL JOURNAL C

Regular Article - Theoretical Physics

NANOGrav signal from double-inflection-point inflation and dark matter

Tie-Jun Gao[a]

School of Physics, Xidian University, Xi'an 710071, China

Received: 24 April 2023 / Accepted: 20 June 2023 / Published online: 25 August 2023

Abstract The NANOGrav collaboration has published a suspected stochastic gravitational wave (GW) background signal in its analysis of 12.5 years PTA data, so in this work, we investigate the possibility to explain the signal by the inflationary models with double-inflection-point. We calculate the energy spectrum of GWs induced by scalar perturbations, and show that the curve lies in the 2σ region of the NANOGrav constraints. In addition, we analyze the reheating process and dark matter production by assuming that the inflaton is coupled with the standard model (SM) Higgs boson and singlet fermionic dark matter field. We discuss the radiative stability of the inflationary potential under one-loop corrections, calculate the reheating temperature, the dark matter production, and constraints on the coupling parameters using the bounds of BBN, Lyman-α, etc.

1 Introduction

Recently, the North American Nanohertz Observatory for Gravitational Waves (NANOGrav) has published its 12.5 years observation data of pulsar timing array (PTA), where strong evidence of a stochastic process, which can be explained by the stochastic gravitational waves (GWs) with a power-law spectrum $\Omega_{GW} \propto f^{5-\gamma}$ at a reference frequency of $f_{yr} \simeq 3.1 \times 10^{-8}$Hz, with the exponent $5-\gamma \in (-1.5, 0.5)$ at 1σ confidence level [1–7].

It has been pointed out in several literatures that if the power spectrum of scalar perturbations has a large peak at low scales, then when the perturbations corresponding to the peak renters the horizon during the radiation-dominated period, it will induce GWs, which is sizable to be detectable by experiments in near future [8–22]. Such enhancement of the power spectrum can be achieved in the ultra-slow-roll phase near the inflection point in some inflationary models [23–28], and similar models have been discussed in many literatures [29–31],or in the framework of string theory [32–35] etc. However, In the previous models, the potential contains single inflection point, and the inflation will last about more than 30 e-folding numbers before the inflection point. Thus near the inflection point, the peak of the power spectrum will induce GWs around millihertz, which couldn't explain the NANOGrav result around nanohertz. So in this paper, motivated from the framework of effective field theory, we consider a polynomial potential model with double-inflection-point. In such a model, the inflection point at CMB scales can make the predictions consistent with the 2018 data [36] and last about 20 e-folding numbers, thus when the inflaton meets the second inflection point, it will induce GWs with the peak around nanohertz, which can explain the NANOGrav signal.

After inflation ends, the inflaton will oscillate around the minimum of the potential and decay into relativistic particles, which will reheat the universe. So in this paper, we assume that the inflaton can decay into the standard model(SM) Higgs boson or decay into singlet fermions beyond SM, which can be a component of dark matter(DM). In order to ensure that the effect of the added coupling terms do not affect the inflationary dynamics at the CMB scale, and do not affect the GW energy spectrum, we discuss the radiative corrections at one-loop order using the Coleman–Weinberg (CW) formalism [37,38]. We also calculate the reheating temperature and constrain the model parameters using BBN [39–43], Lyman-α [44,45], etc. We also analysis the dark matter production, and show that the main way to produce dark matter is the direct decay of inflatons.

The paper is organized as follows. In the next section, we setup the inflationary model with double-inflection-point using a scalar potential with polynomial form. In Sect. 3, we analyze the inflation dynamics of the model and calculate the power spectrum numerically. In Sect. 4, we calculate

[a] e-mail: tjgao@xidian.edu.cn (corresponding author)

the energy spectrum of the induced GWs and compared the results with NANOGrav and some planned experiments. In Sect. 4, we assume that after inflation, the inflaton will decay into SM Higgs or singlet fermionic field and analyze the reheating temperature. We also calculate the effect of one-loop corrections of the coupling terms in Sect. 5. In Sect. 6, we discuss the dark matter production and calculate the relic density. The last section is devoted to summary.

2 The double-inflection-point model

In this section, we consider a scalar potential with polynomial form, which can generate an inflationary model with double-inflection-point. Such a polynomial can be derived from the effective field theory with a cutoff scale Λ [46–51]

$$V_{\rm eff}(\phi) = \sum_{n=0} \frac{b_n}{n!} \left(\frac{\phi}{\Lambda}\right)^n . \tag{1}$$

To obtain a inflationary potential containing double-inflection-point, we truncate the above polynomial to the sixth order, and redefine the parameters as

$$V(\phi) = V_0 \Bigg[c_2 \left(\frac{\phi}{\Lambda}\right)^2 + c_3 \left(\frac{\phi}{\Lambda}\right)^3 + c_4 \left(\frac{\phi}{\Lambda}\right)^4 + c_5 \left(\frac{\phi}{\Lambda}\right)^5 + \left(\frac{\phi}{\Lambda}\right)^6 \Bigg], \tag{2}$$

where the overall factor V_0 can be constrained by the amplitude of scalar perturbations A_s, and we have omitted the constant and first-order terms of the polynomial so that the potential and it's first-order derivative vanish at the origin. By tuning the four dimensionless parameters c_{2-5} one can obtain a potential with two inflection points.

For the purpose of discussion, we assume that the two inflection points are located at $\phi_i (i = 1, 2)$, where the first and second derivatives of V vanish,i.e. $V'(\phi_i) = 0$ and $V''(\phi_i) = 0$. This condition yields the following relationship between c_{2-5} and ϕ_i

$$c_2 = \frac{3}{\Lambda^4}\phi_1^2\phi_2^2,\ c_3 = \frac{-4}{\Lambda^3}\left(\phi_1^2\phi_2 + \phi_1\phi_2^2\right),$$
$$c_4 = \frac{3}{2\Lambda^2}\left(\phi_1^2 + 4\phi_1\phi_2 + \phi_2^2\right),\ c_5 = \frac{-12}{5\Lambda}(\phi_1 + \phi_2). \tag{3}$$

However, in order to obtain a reasonable model, the inflection points of the potential are not strict, so we introduce two additional parameters α_i to represent the small deviation. Then the scalar potential can be written in the following form

$$V(\phi) = \frac{V_0}{\Lambda^6}\Big(3\phi_1^2\phi_2^2\phi^2 - 4\left(\phi_1^2\phi_2 + \phi_1\phi_2^2\right)(1+\alpha_1)\phi^3 + \frac{3}{2}\left(\phi_1^2 + 4\phi_1\phi_2 + \phi_2^2\right)\phi^4 - \frac{12}{5}(\phi_1 + \phi_2)(1+\alpha_2)\phi^5 + \phi^6\Big). \tag{4}$$

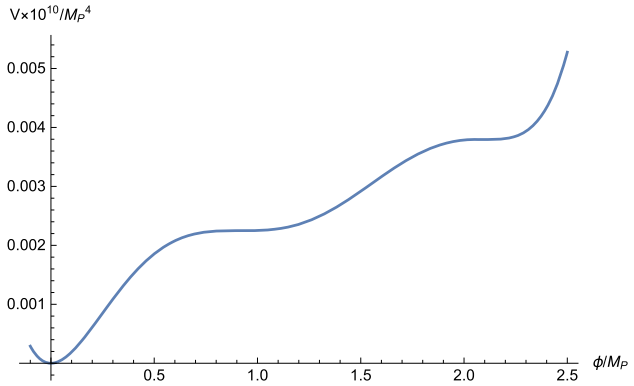

Fig. 1 The scalar potential with parameter set (5)

For some parameter spaces, the model is both consistent with the CMB observational constraints and interprets the NANOGrav signal. For instance, we choose

$$V_0 = 2.157 \times 10^{-13} M_p^4, \quad \Lambda = M_p,$$
$$\phi_1 = 0.9095875 M_p, \quad \alpha_1 = 8.5654 \times 10^{-5},$$
$$\phi_2 = 2.10081 M_p, \quad \alpha_2 = -4.0172 \times 10^{-5}, \tag{5}$$

which corresponds to the parameters c_{2-5} are

$$c_2 = 10.9543,\ c_3 = -23.0119,\ c_4 = 19.3264,$$
$$c_5 = -7.22466. \tag{6}$$

In Fig. 1 we draw the corresponding potential, which contains double-inflection-point.

As we will see below, the inflation starts near the first inflection point at high scale and generates a nearly scale-invariant power spectrum, which is in good agreement with the CMB observations, and when the inflaton rolls near the second inflection point at low scale, it will go through an ultra-slow-roll phase, which will last about 35 e-folding numbers and resulting in a large peak in the power spectrum, which will induce gravitational waves consistent with the NANOGrav data.

3 Inflation dynamics

In this section, we will discuss the dynamics of inflation. Since there is an ultra-slow-roll stage in the process of inflation, so in order to calculate the power spectrum more accurately, we use the Hubble slow roll parameters defined below [52–58]

$$\epsilon_H = -\frac{\dot{H}}{H^2},$$
$$\eta_H = -\frac{\ddot{H}}{2H\dot{H}} = \epsilon_H - \frac{1}{2}\frac{d\ln\epsilon_H}{dN_e}, \tag{7}$$

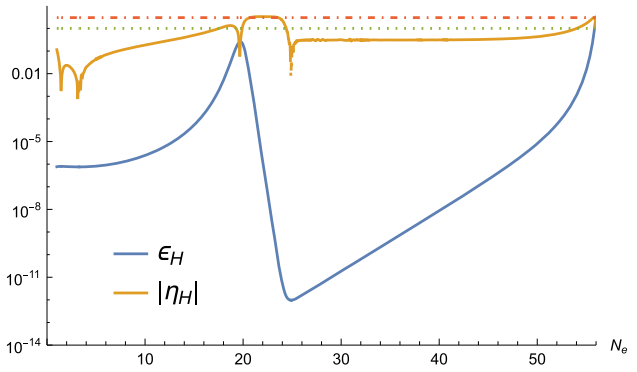

Fig. 2 The Hubble slow-roll parameters ϵ_H and η_H as functions of the e-folding number N_e. The green and red dashed lines represent 1 and 3, respectively

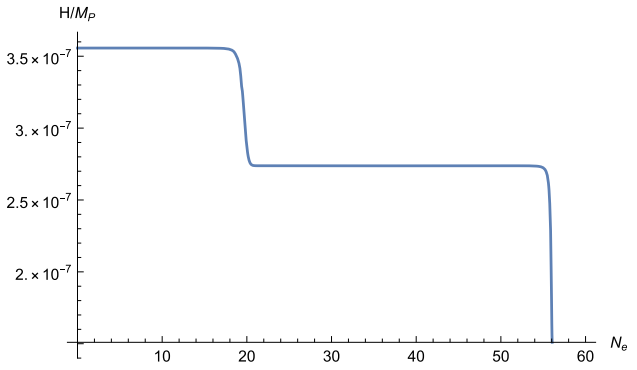

Fig. 3 The Hubble parameters as functions of the e-folding number N_e

with dots represent derivatives with respect to the cosmic time, and N_e is the e-folding numbers. The corresponding curves of ϵ_H and η_H with respect to N_e are shown in Fig. 2, and the evolution of Hubble parameter with respect to N_e are shown in Fig. 3.

As we can see in the figure, near the second inflection point, the slow-roll parameter $|\eta_H| > 3$, which implies that inflation undergoes an ultra-slow-roll process. Correspondingly, the curve of the slow-roll parameter ϵ_H appears a deep valley lasting about 30 e-folding numbers, which will make the power spectrum appear a large peak. In order to calculate the power spectrum at the ultra-slow-roll process, the slow-roll approximation is no longer applicable, so the Mukhanov–Sasaki(MS) equation of mode function u_k, must be solved strictly [26]

$$\frac{d^2u_k}{d\tau^2} + \left(k^2 - \frac{1}{z}\frac{d^2z}{d\tau^2}\right)u_k = 0, \tag{8}$$

with $z \equiv \frac{a}{\mathcal{H}}\frac{d\phi}{d\tau}$, and τ denotes the conformal time. And the initial condition is taken to be the Bunch-Davies type [59]

$$u_k \to \frac{e^{-ik\tau}}{\sqrt{2k}}, \quad \text{as} \quad \frac{k}{aH} \to \infty. \tag{9}$$

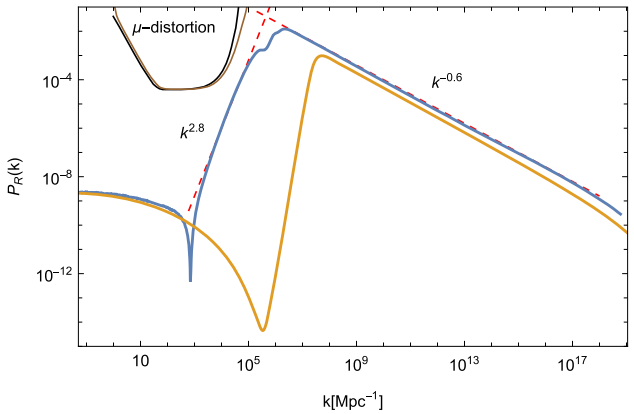

Fig. 4 The power spectrum of scalar perturbations with the parameter set (5). And the black and brown lines show the upper bound from μ-distortion for a delta function power spectrum and for the steepest growth k^4 power spectrum, respectively [60]

Then the power spectrum are calculated by

$$\mathcal{P}_\mathcal{R} = \frac{k^3}{2\pi^2}\left|\frac{u_k}{z}\right|^2_{k\ll aH}. \tag{10}$$

We show the numerical result(blue line) and the approximate results(orange line) of the scalar power spectrum in Fig. 4. And the constraints on the primordial power spectrum from μ-distortion of CMB are also show there.

We can see that the ultra-slow-roll behavior near the inflection point leads to a large peak in the power spectrum, and the peak value is about seven orders of magnitude higher than the power spectrum of the CMB scale. We will see in the next section that the perturbations corresponding to the peak will induce experimentally detected GWs after re-entering the horizon, and can explain the signal of NANOGrav.

In order to verify that the model agrees with the constraints of Planck experiment on CMB scale, we estimate the corresponding scalar spectral index and the tensor-to-scalar ratio, which can be expressed using ϵ_H and η_H at the leading order as

$$\begin{aligned} n_s &= 1 - 4\epsilon_H + 2\eta_H, \\ r &= 16\epsilon_H. \end{aligned} \tag{11}$$

The numerical results are $n_s = 0.9672$, $r = 1.22 \times 10^{-5}$, and the amplitude of the primordial curvature perturbations A_s and the e-folding numbers during inflation N_e are $\ln(10^{10}A_s) = 3.0444$, $N_e = 56.6$. The results are all consistent with the observation constraints from Planck 2018, which are $n_s = 0.9649 \pm 0.0042$, $r < 0.064$ and $\ln(10^{10}A_s) = 3.044 \pm 0.014$ [36].

4 Induced gravitational waves

In the following, we will numerical calculate the second order GWs induced by scalar perturbations using the power spectrum obtained in the province subsection. When the scalar perturbation re-enters the horizon, it will induce second-order GWs [61–66], and the corresponding GW energy spectrum can be expressed by the tensor power spectrum as

$$\Omega_{\rm GW}(\tau,k)=\frac{1}{24}\left(\frac{k}{\mathcal{H}}\right)^2\overline{\mathcal{P}_h(\tau,k)}, \tag{12}$$

where the overline denotes the oscillation averaged among several wavelengths. Using the Green's function method and considering that $\mathcal{H}=1/\tau$ in the radiation dominant period, the above energy spectrum can be calculated by the scalar power spectrum as following [13]

$$\begin{aligned}\Omega_{\rm GW}(\tau,k)=&\frac{1}{12}\int_0^\infty dv\int_{|1-v|}^{1+v}du\left(\frac{4v^2-\left(1+v^2-u^2\right)^2}{4uv}\right)^2\\&\times\mathcal{P}_{\mathcal{R}}(ku)\mathcal{P}_{\mathcal{R}}(kv)\\&\times\left(\frac{3}{4u^3v^3}\right)^2\left(u^2+v^2-3\right)^2\\&\times\left\{\left[-4uv+\left(u^2+v^2-3\right)\ln\left|\frac{3-(u+v)^2}{3-(u-v)^2}\right|\right]^2\right.\\&\left.+\left[\pi\left(u^2+v^2-3\right)\Theta(u+v-\sqrt{3})\right]^2\right\},\end{aligned} \tag{13}$$

where u and v are two dimensionless variables. Finally, the energy density spectrum of GWs today $\Omega_{\rm GW,0}$ is calculated by [63]

$$\Omega_{\rm GW,0}=0.83\left(\frac{g_*}{g_{*,p}}\right)^{-1/3}\Omega_{r,0}\Omega_{\rm GW}, \tag{14}$$

with $\Omega_{r,0}\simeq 9.1\times10^{-5}$ is the energy density fraction of radiation at present, g_* and $g_{*,p}$ denote the effective number of degrees of freedom for energy density today and at the horizon crossing, respectively.

Combine the numerical result of scalar power spectrum $\mathcal{P}_{\mathcal{R}}$ obtained in the previous subsection, we numerically calculate the energy spectrum of induced GWs and show it in Fig. 5, with the horizontal axis is the frequency at present

$$f\approx0.03{\rm Hz}\frac{k}{2\times10^7{\rm pc}^{-1}}. \tag{15}$$

And the upper curves are the sensitivity curves of some planned GW detectors [31,67–71].

Recently, the NANOGrav collaboration has published its 12.5-year data of PTA, which indicate a signal which can be explained by the stochastic GWs with a power-law spectrum around $f_{yr}\simeq3.1\times10^{-8}$Hz,

$$\Omega_{GW}(f)=\frac{2\pi^2f_{yr}^2}{3H_0^2}A_{GWB}^2\left(\frac{f}{f_{yr}}\right)^{5-\gamma}, \tag{16}$$

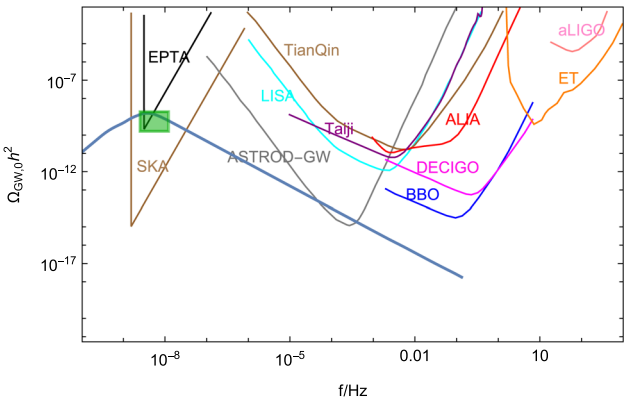

Fig. 5 Energy spectrum of the induced GWs at the present time predicted by the polynomial model for parameter set (5). The curves in the upper part are the expected sensitivity curves of the European pulsar timing array (EPTA), square kilometer array (SKA), laser interferometer space antenna (LISA),Taiji, TianQin, astrodynamical space test of relativity using optical-GW detector (ASTROD-GW), advanced laser interferometer antenna (ALIA), big bang observer (BBO), deci-hertz interferometer GW observatory (DECIGO), Einstein telescope (ET), advanced LIGO (aLIGO), respectively. These sensitivity curves are taken from Refs. [31,67–71] The green region show the 2σ confidence level of the NANOGrav results with the tilt of $5-\gamma=0$ [1]

where $H_0\equiv100h$ km/s/Mpc, and $5-\gamma\in(-1.5,0.5)$ at 1σ confidence level [1–7]. The observed GWs for $5-\gamma=0$ with 2σ uncertainty on A_{GWB} are also show in Fig. 5.

We can see that the frequencies of the spectrum of GWs cover from nanohertz to millihertz, and the maximum is at the frequency $f=3.97\times10^{-9}Hz$, which is within the frequency range of SKA and EPTA. The spectrum of induced GWs with frequencies around nanohertz lies in the 2σ region of the NANOGrav constraints, so it can explain the NANOGrav signals. And around millihertz, the energy spectrum curves lies above the expected sensitivity curves of ASTROD-GW, so it can be tested by the observation in near future.

Moreover, we also zoom in Fig. 5 around NANOGrav's frequency range and show the energy spectrum of the induced GWs with different parameters in Fig. 6. We can see from Fig. 6(a) that the energy spectrum decrease as ϕ_1 increase from $0.9095873M_p$ to $0.9095875M_p$, in Fig. 6(b), the energy spectrum increase as ϕ_2 increase from $2.100810M_p$ to $2.100811M_p$, and from Fig. 6(c), (d), we can see that the energy spectrum decrease as α_1 increase from 8.5652×10^{-5} to 8.5654×10^{-5}, and decrease as α_2 increase from -4.0172×10^{-5} to -4.0174×10^{-5}.

5 Reheating

After inflation ends, the inflaton rolls down the potential and then oscillates around the minimum, and the energy of inflaton will transfer to other degree of freedoms and raises the

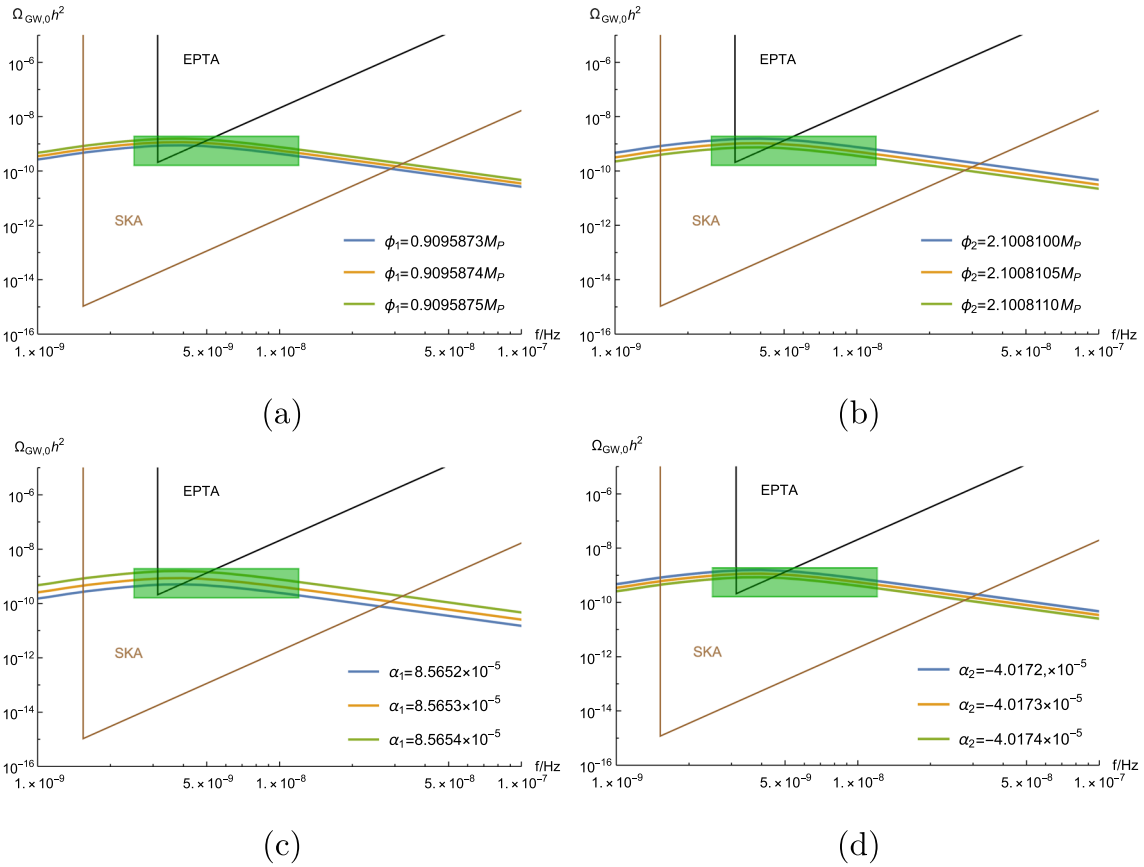

Fig. 6 The zoom in version of Fig. 5 around nanohertz frequency. Where the parameters ϕ_1 increase from $0.9095873M_p$ to $0.9095875M_p$ in (**a**), ϕ_2 increase from $2.100810M_p$ to $2.100811M_p$ in (**b**), α_1 increase from 8.5652×10^{-5} to 8.5654×10^{-5} in (**c**) and α_2 increase from -4.0172×10^{-5} to -4.0174×10^{-5} in (**d**), respectively

temperature of the universe. This is known as the reheating period. Following References [72–74], we consider the inflaton decays into SM Higgs boson or decays into a Dirac fermion χ through trilinear coupling, which can be a candidate of DM. The additional terms in the Lagrangian density has the following form

$$\begin{aligned}\mathcal{L} &= i\bar{\chi}\gamma^\mu\partial_\mu\chi - m_\chi\bar{\chi}\chi - y_\chi\phi\bar{\chi}\chi - \lambda_{12}\phi H^\dagger H \\ &\quad -\frac{1}{2}\lambda_{22}\phi^2 H^\dagger H,\end{aligned} \tag{17}$$

where m_χ is the mass of the DM, the coupling coefficient y_χ, λ_{22} are dimensionless and λ_{12} has a dimension of mass. The associated decay widths are

$$\begin{aligned}\Gamma_{\phi\to H^\dagger H} &\simeq \frac{\lambda_{12}^2}{8\pi m_\phi}, \\ \Gamma_{\phi\to\bar{\chi}\chi} &\simeq \frac{y_\chi^2 m_\phi}{8\pi},\end{aligned} \tag{18}$$

with $m_\phi^2 = \frac{\partial^2 V}{\partial\phi^2}|_{\phi=0}$ is the inflaton mass during reheating, and we have assumed that the mass of χ and H are much smaller than m_ϕ. In order to fit the relic density of photon numbers and hadronic numbers today, the decay width to the SM Higgs boson should be much greater than the decay width to the fermionic DM, that is the total decay width of the inflaton be approximated as $\Gamma \equiv \Gamma_{\phi\to H^\dagger H} + \Gamma_{\phi\to\bar{\chi}\chi} \simeq \Gamma_{\phi\to H^\dagger H}$. Therefore branching ratio of DM production can be calculated as follows

$$\mathrm{Br} \equiv \frac{\Gamma_{\phi\to\bar{\chi}\chi}}{\Gamma_{\phi\to H^\dagger H} + \Gamma_{\phi\to\bar{\chi}\chi}} \simeq \frac{\Gamma_{\phi\to\bar{\chi}\chi}}{\Gamma_{\phi\to H^\dagger H}} \simeq m_\phi^2\left(\frac{y_\chi^2}{\lambda_{12}^2}\right). \tag{19}$$

During reheating, when the Hubble parameter becomes small enough, the energy loss due to the decay of the inflaton is greater than the energy loss due to the expansion of the universe, the corresponding temperature when $H = \frac{2}{3}\Gamma$ is defined as the reheating temperature T_{rh}. In the instantaneous decay approximation the reheating temperature can be calculated as [73]

$$T_{rh} = \sqrt{\frac{2}{\pi}}\left(\frac{10}{g_*}\right)^{1/4}\sqrt{M_P}\sqrt{\Gamma}, \tag{20}$$

where Γ is the total decay width of the inflaton, and $g_* = 106.75$. And the maximum temperature during reheating can

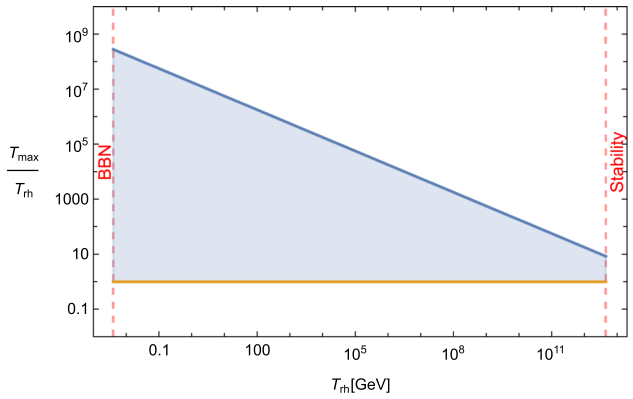

Fig. 7 The allowed ranges of the ratio $T_{\max}/T_{rh}$

be calculated by [75–77]

$$T_{\max} = \Gamma^{1/4}\left(\frac{60}{g_*\pi^2}\right)^{1/4}\left(\frac{3}{8}\right)^{2/5} H_I^{1/4} M_P^{1/2}, \tag{21}$$

where H_I is the Hubble parameter at the beginning of reheating. In our model, according to Fig. 3, we use the value around the second inflection point.

According to the restriction of BBN, the reheating temperature T_{rh} should be greater than 4MeV [39–43]. Moreover, the Planck 2018 give an upper limit on the inflation scale $H_I \leq 2.5 \times 10^{-5} M_p$ [36], which would allows an upper limit on the reheating temperature $T_{rh} \leq 7 \times 10^{15}$GeV. So we can give the limit of the coupling parameter λ_{12} according to Eq. (20)

$$2.7451 \times 10^{-23} \leq \frac{\lambda_{12}}{M_p} \leq 4.8039 \times 10^{-5}. \tag{22}$$

In addition, we estimate the value of $T_{\max}/T_{rh}$

$$\frac{T_{\max}}{T_{rh}} = \left(\frac{3}{8}\right)^{2/5}\left(\frac{3M_p}{\pi}\sqrt{\frac{10}{g_*}}\frac{\mathcal{H}_I}{T_{rh}^2}\right)^{1/4}, \tag{23}$$

and show the allowed ranges in Fig. 7. Where the lower bound of T_{rh} is from the BBN $T_{rh} > 4MeV$ and the upper bound is from the stability discussed in the next section, $T_{rh} < 4.43 \times 10^{12}$GeV.

6 Radiative corrections and stability

In order to ensure that the coupling terms added in the discussion of the reheating process in the previous section do not affect the inflationary dynamics at the CMB scale, and do not affect the generation of GWs at the second inflection point, thus do not affect the parameter space of the model, we analysis the stability of the inflation potential, calculate the one-loop CW correction of these coupling terms to the inflationary potential and restrict the coupling parameters.

The one-loop CW correction is [37,38]

$$\Delta V = \sum_j \frac{g_j}{64\pi^2}(-1)^{2s_j}\tilde{m}_j^4\left[\ln\left(\frac{\tilde{m}_j^2}{\mu^2}\right) - \frac{3}{2}\right], \tag{24}$$

and the corresponding first and second derivative of V_{CW} are

$$\begin{aligned} V'_{\rm CW} &= \sum_j \frac{g_j}{32\pi^2}(-1)^{2s_j}\tilde{m}_j^2\left(\tilde{m}_j^2\right)'\left[\ln\left(\frac{\tilde{m}_j^2}{\mu^2}\right) - 1\right], \\ V''_{\rm CW} &= \sum_j \frac{g_j}{32\pi^2}(-1)^{2s_j}\left\{\left[\left(\left(\tilde{m}_j^2\right)'\right)^2 + \tilde{m}_j^2\left(\tilde{m}_j^2\right)''\right]\right. \\ &\quad \left.\times \ln\left(\frac{\tilde{m}_j^2}{\mu^2}\right) - \tilde{m}_j^2\left(\tilde{m}_j^2\right)''\right\}, \end{aligned} \tag{25}$$

where the index j is summing over three fields, the inflaton, the Higgs H and the fermion χ, and the spin s_j are $s_H = 0, s_\chi = 1/2, s_\phi = 0$,the number of degrees of freedom of the fields are $g_H = 4, g_\chi = 4, g_\phi = 0$, respectively. The renormalization scale μ is taken as ϕ_0. $\tilde{m}_j$ are field-dependent masses, and in our model they are given by

$$\begin{aligned} \tilde{m}_\phi^2(\phi) &= \frac{6V_0}{\Lambda^6}\left(5\phi^4 - 8(\alpha_2+1)\phi^3(\phi_1+\phi_2)\right. \\ &\quad +3\phi^2\left(\phi_1^2 + 4\phi_1\phi_2 + \phi_2^2\right) \\ &\quad \left.-4(\alpha_1+1)\phi\phi_1\phi_2(\phi_1+\phi_2) + \phi_1^2\phi_2^2\right), \\ \tilde{m}_\chi^2(\phi) &= \left(m_\chi + y_\chi\phi\right)^2, \\ \tilde{m}_H^2(\phi) &= m_H^2 + \lambda_{12}\phi. \end{aligned} \tag{26}$$

At the high scale inflection point ϕ_2, the first and second derivatives of inflation potential are

$$\begin{aligned} V'(\phi_2) &= -\frac{12V_0}{\Lambda^6}{\phi_2}^3(\phi_1+\phi_2)(\alpha_1\phi_1 + \alpha_2\phi_2), \\ V''(\phi_2) &= -\frac{24V_0}{\Lambda^6}{\phi_2}^2(\phi_1+\phi_2)(\alpha_1\phi_1 + 2\alpha_2\phi_2), \end{aligned} \tag{27}$$

and at such point, the derivatives of the one-loop CW correction are

$$\begin{aligned} V'_{CW}(\phi_2) &= \frac{\lambda_{12}^2\phi_2(\ln\left(\frac{\lambda_{12}}{\phi_2}\right) - 1) - 2{\phi_2}^3 y_\chi^4(\ln\left(y_\chi^2\right) - 1)}{8\pi^2} \\ &\quad +\frac{1}{\pi^2\Lambda^{12}}9{V_0}^2{\phi_2}^3 \\ &\quad \times\left(\ln\left(-\frac{24V_0(\phi_1+\phi_2)(\alpha_1\phi_1+2\alpha_2\phi_3)}{\Lambda^6}\right) - 1\right) \\ &\quad \times(\phi_1+\phi_2)(\alpha_1\phi_1+2\alpha_2\phi_2) \\ &\quad \times((2\alpha_1-1){\phi_1}^2 + 2(1+\alpha_1+6\alpha_2)\phi_1\phi_2 \\ &\quad +(12\alpha_2-1){\phi_2}^2), \\ V''_{CW}(\phi_2) &= \frac{\lambda_{12}^2\ln\left(\frac{\lambda_{12}}{\phi_2}\right) + 2{\phi_2}^2 y_\chi^4(1 - 3\ln\left(y_\chi^2\right))}{8\pi^2} \end{aligned}$$

$$
\begin{aligned}
&+\frac{1}{4\pi^2\Lambda^{12}}9{V_0}^2{\phi_2}^2\\
&\times\Big(3((1-2\alpha_1){\phi_1}^2-2(1+\alpha_1+6\alpha_2)\phi_1\phi_2\\
&+(1-12\alpha_2){\phi_2}^2)^2-6(\phi_1+\phi_2)(\alpha_1\phi_1+2\alpha_2\phi_2)({\phi_1}^2\\
&+(3-8\alpha_2){\phi_2}^2-4\phi_1(\phi_2+2\alpha_2\phi_2))\\
&+2((1-2\alpha_1){\phi_1}^2-2(1+\alpha_1+6\alpha_2)\phi_1\phi_2\\
&+(1-12\alpha_2){\phi_2}^2)^2\\
&\times\left(\ln\left(-\frac{24V_0(\phi_1+\phi_2)(\alpha_1\phi_1+2\alpha_2\phi_2)}{\Lambda^6}\right)-\frac{3}{2}\right)\\
&-6(\phi_1+\phi_2)(\alpha_1\phi_1+2\alpha_2\phi_2)({\phi_1}^2\\
&+(3-8\alpha_2){\phi_2}^2-4\phi_1(\phi_2+2\alpha_2\phi_2))\\
&\times\left(2\ln\left(-\frac{24V_0(\phi_1+\phi_2)(\alpha_1\phi_1+2\alpha_2\phi_2)}{\Lambda^6}\right)-3\right)\Big).
\end{aligned}
\tag{28}
$$

In order to make sure the addition coupling terms do not affect the inflation dynamics, we need to make sure that the terms of y_χ^4 and λ_{12}^2 are much smaller than the tree-level results (27), which will give the following restrictions on the parameters spaces

$$
\begin{aligned}
y_\chi &< 1.00687\times10^{-4},\\
\lambda_{12} &< 3.03996\times10^{-8}M_p,\\
y_\chi &< 1.8046\times10^{-4},\\
\lambda_{12} &< 1.73968\times10^{-7}M_p.
\end{aligned}
\tag{29}
$$

In addition, in our model we must also need to ensure that the addition coupled terms will not affect the generation of GWs, that is, the corresponding terms of y_χ^4 and λ_{12}^2 in the one-loop CW corrections at the low scale inflection point

$$
\begin{aligned}
V'_{CW}(\phi_2) &= \frac{{\lambda_{12}}^2\phi_1\left(\ln\left(\frac{\lambda_{12}}{\phi_1}\right)-1\right)-2{\phi_1}^3\left(\ln\left(y_\chi^2\right)-1\right)y_\chi^4}{8\pi^2}\\
&+\frac{1}{\pi^2\Lambda^{12}}9{V_0}^2{\phi_1}^3\left(\ln\left(-\frac{24V_0(\phi_1+\phi_2)(2\alpha_2\phi_1+\alpha_1\phi_2)}{\Lambda^6}\right)-1\right)\\
&\times(\phi_1+\phi_2)(2\alpha_2\phi_1+\alpha_1\phi_2)\\
&\times((12\alpha_2-1){\phi_1}^2+2(1+\alpha_1+6\alpha_2)\phi_1\phi_2+(2\alpha_1-1){\phi_2}^2),\\
V''_{CW}(\phi_2) &= \frac{({\lambda_{12}}^2\ln\left(\frac{\lambda_{12}}{\phi_1}\right)-2{\phi_1}^2(3\ln\left(y_\chi^2\right)-1)y_\chi^4)}{8\pi^2}\\
&+\frac{1}{4\pi^2\Lambda^{12}}9{V_0}^2{\phi_1}^2\\
&\times\big(3((1-12\alpha_2){\phi_1}^2-2(1+\alpha_1+6\alpha_2)\phi_1\phi_2+(1-2\alpha_1){\phi_2}^2)^2\\
&+6(\phi_1+\phi_2)(2\alpha_2\phi_1+\alpha_1\phi_2)((-3+8\alpha_2){\phi_1}^2-{\phi_2}^2\\
&.+4\phi_1(\phi_2+2\alpha_2\phi_2))\\
&+2((1-12\alpha_2){\phi_1}^2-2(1+\alpha_1+6\alpha_2)\phi_1\phi_2+(1-2\alpha_1){\phi_2}^2)^2\\
&\times(\ln\left(-\frac{24V_0(\phi_1+\phi_2)(2\alpha_2\phi_1+\alpha_1\phi_2)}{\Lambda^6}\right)-\frac{3}{2})\\
&+6(\phi_1+\phi_2)(2\alpha_2\phi_1+\alpha_1\phi_2)((-3+8\alpha_2){\phi_1}^2-{\phi_2}^2\\
&+4\phi_1(\phi_2+2\alpha_2\phi_2))\\
&\times(2\ln\left(-\frac{24V_0(\phi_1+\phi_2)(2\alpha_2\phi_1+\alpha_1\phi_2)}{\Lambda^6}\right)-3)\big),
\end{aligned}
\tag{30}
$$

are much smaller than the terms of tree-level

$$
\begin{aligned}
V'(\phi_1) &= -\frac{12V_0}{\Lambda^6}{\phi_1}^3(\phi_1+\phi_2)(\alpha_2\phi_1+\alpha_1\phi_2),\\
V''(\phi_1) &= -\frac{24V_0}{\Lambda^6}{\phi_1}^2(\phi_1+\phi_2)(2\alpha_2\phi_1+\alpha_1\phi_2),
\end{aligned}
\tag{31}
$$

which will give the following restrictions

$$
\begin{aligned}
y_\chi &< 2.2307\times10^{-4},\\
\lambda_{12} &< 6.46594\times10^{-8}M_p,\\
y_\chi &< 1.88144\times10^{-4},\\
\lambda_{12} &< 8.18895\times10^{-8}M_p.
\end{aligned}
\tag{32}
$$

Combine (29) and (32), we get the upper bounds are $y_\chi < 1.00687\times10^{-4}$ and $\lambda_{12} < 3.03996\times10^{-8}M_p$. Plugging the upper limit of λ_{12} into (20), we can give an upper limit on the reheating temperature $T_{rh} < 4.43\times10^{12}$GeV.

7 Dark matter production and relic density

In this section, we will study dark matter production during reheating. Combining the Boltzmann equation of DM number density n_χ and the Friedman equation, and considering that during $T_{rh} < T < T_{max}$ the energy density is dominated by the inflaton, then we can obtain the following relationship between the comoving number density $N = n_\chi a^3$ of DM and the reheating temperature T_{rh} as [73]

$$
\frac{dN}{dT} = -\frac{8}{\pi}\sqrt{\frac{10}{g_*}}\frac{M_pT_{\rm rh}^{10}}{T^{13}}a^3\,(T_{\rm rh})\,\gamma,
\tag{33}
$$

where a is the scale factor and γ is the density of DM production rate. And then the DM yield $Y \equiv n_\chi/s$ can be expressed as

$$
\frac{dY}{dT} = -\frac{135}{2\pi^3g_{*,s}}\sqrt{\frac{10}{g_*}}\frac{M_p}{T^6}\gamma,
\tag{34}
$$

where $s \equiv \frac{2\pi^2}{45}g_{*,s}T^3$is the entropy density at temperature T, and $g_{*,s}$ is the number of relativistic degrees of freedom contributing to the SM entropy [78]. In addition, it is worth to note that in order to consistent with observations of DM energy density, the present day DM yield is fixed by [73]

$$
m_\chi Y_0 \simeq 4.3\times10^{-10}\text{GeV}.
\tag{35}
$$

After inflation, the DM can produced by the direct decay of inflatons, the 2-to-2 scattering of inflatons and the 2-to-2 scattering of SM particles.

The main way of dark matter production is the direct decay of inflatons, in this case, the DM production rate density is

$$
\gamma = 2\text{Br}\Gamma\frac{\rho}{m}.
\tag{36}
$$

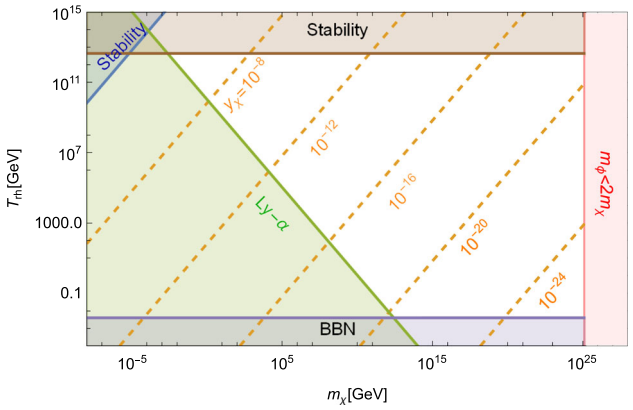

Fig. 8 The allowed range of coupling parameters y_χ when the direct decay of the inflaton produces the whole DM

Using Eq. (34), we can get that the corresponding DM yield in this case is

$$Y_0 \simeq \frac{3}{\pi}\frac{g_*}{g_{*,s}}\sqrt{\frac{10}{g_*}}\frac{M_p\Gamma}{m_\phi T_{\rm rh}}$$
$$\mathrm{Br} \simeq 1.163\times 10^{-2} M_p \frac{y_\chi^2}{T_{rh}}, \tag{37}$$

In the above equation we have assume that $g_{*,s} = g_*$. Combined with Eq. (35), we obtain the conditions if the inflatons decay constitutes the whole DM abundance, and show the allowed range of the coupling coefficient y_χ in Fig. 8.

Where the constraints of purple region is from the BBN, $T_{rh} > 4MeV$. The brown region $T_{rh} < 4.43\times 10^{12}$Gev and the blue region $y_\chi < 1.00687\times 10^{-4}$ are all from the discussion of stability in Sect. 6, the green region is from the $Lyman-\alpha$ bound $\frac{m_\chi}{keV} \geq \frac{2m_\phi}{T_{rh}}$ [73], the red region is from the kinematical threshold $m_\phi > 2m_\chi$. From Fig. 8 we can further get that if inflatons decay process constitutes all the DM, the parameter y_χ should satisfies $2.081\times 10^{-27} < y_\chi < 5.294\times 10^{-6}$.

Secondly, dark matter can be produced by the 2-to-2 scatter of the inflaton. In this case [79–81]

$$\gamma = \frac{\pi^3 g_*^2}{3686400}\frac{T^{16}}{M_p^4 T_{\rm rh}^8}\frac{m_\chi^2}{m_\phi^2}\left(1-\frac{m_\chi^2}{m_\phi^2}\right)^{3/2}, \tag{38}$$

and the the corresponding DM yield is

$$Y_0 \simeq \frac{g_*^2}{81920 g_{*,s}}\sqrt{\frac{10}{g_*}}\left(\frac{T_{\rm rh}}{M_p}\right)^3\left[\left(\frac{T_{\rm max}}{T_{\rm rh}}\right)^4-1\right]\frac{m_\chi^2}{m_\phi^2}$$
$$\times\left(1-\frac{m_\chi^2}{m_\phi^2}\right)^{3/2}$$
$$\simeq 1.8\times 10^{-2}\frac{T_{\rm rh} m_\chi^2}{M_p^{5/2} m_\phi^{1/2}}\left(1-\frac{m_\chi^2}{m_\phi^2}\right)^{3/2}. \tag{39}$$

Combine with the upper bound of $T_{rh} < 4.43\times 10^{12}$GeV in Sect. 6, we get that for reasonable values of m_χ, the DM yield Y_0 is less than 10^{-18}, the contribution to DM abundance is negligible.

Thirdly, dark matter can also be produced via the 2-to-2 scattering of SM particles, mediated by gravitons or inflatons. For gravitons act as mediators, one can get the decay rate density is [82–84]

$$\gamma(T) = \alpha\frac{T^8}{M_p^4}, \tag{40}$$

with $\alpha \simeq 1.1\times 10^{-3}$. The corresponding DM Yield through this channel is

$$Y_0 = \begin{cases} \frac{45\alpha}{2\pi^3 g_{*,s}}\sqrt{\frac{10}{g_*}}\left(\frac{T_{rh}}{M_p}\right)^3, & \text{for } m_\chi \ll T_{rh}, \\ \frac{45\alpha}{2\pi^3 g_{*,s}}\sqrt{\frac{10}{g_*}}\frac{T_{rh}^7}{M_p^3 m_\chi^4}, & \text{for } T_{rh} \ll m_\chi \ll T_{\rm max}. \end{cases} \tag{41}$$

Similarly, if the mediators are inflatons, we can get

$$\gamma(T) \simeq \frac{y_\chi^2\lambda_{12}^2}{2\pi^5}\frac{T^6}{m_\phi^4}, \tag{42}$$

and the dark matter Yield is

$$Y_0 \simeq \frac{135 y_\chi^2\lambda_{12}^2}{4\pi^8 g_{*,s}}\sqrt{\frac{10}{g_*}}\frac{M_p T_{rh}}{m_\phi^4}, \quad \text{for } T_{rh} \ll m_\phi. \tag{43}$$

Using the upper bound of y_χ, λ_{12} and T_{rh} in Sect. 6, we carry out numerical calculation on Y_0, and for the graviton mediation the maximum value is on the order of $Y_0 \sim 10^{-23}$ for $m_\chi \ll T_{rh}$, $Y_0 \sim 10^{-25}$ for $T_{rh} \ll m_\chi \ll T_{\rm max}$, and for the inflatons as the mediators, the maximum value is $Y_0 \sim 10^{-48}$, which are all very small compared to the present DM density, so that we can ignore both cases of the 2-to-2 scattering processes. In addition, we also estimate the rate of annihilation of dark matter into Higgs $\bar{\chi}\chi \to H^\dagger H$ with inflatons acting as the mediator, and find that for the entire parameter space, if we take the upper bound of y_χ and λ_{12}, the maximum of the rate is about 2.21×10^{-65} at the present time, which is too small to be detected in near future.

Moreover, when the scalar perturbations corresponding to the peak of the power spectrum renter the horizon, it will produce the primordial black hole (PBHs) through gravitational collapse, which could also be a candidate of DM [85–90]. Thus we also calculate the abundance of PBHs using the Press-Schechter approach of gravitational collapse, and found that the peak mass of PBHs is around $0.7M_\odot$ and the fraction in dark matter is about 10^{-33}, which is very small and can be negligible.

8 Summary

In this paper we discuss the explanation of NANOGrav data using inflationary potential with double-inflection-point, and such potential can be realized by the polynomial potential from effective field theory with a cut off scale. For some choices of parameter sets, we analyze the inflation dynamics and show that the inflection point at the high scale predicts a scale-invariant power spectrum which is consistent with the observations of the CMB. On the other hand, the inflection point at the low scale can cause an ultra-slow-roll stage, which will generate a peak in the scalar power spectrum, the height of which is about 10^7 magnitude of the CMB scale power spectrum. When the perturbations corresponding to the peak value re-enters the horizon, it will induce GWs that can be detected by experiments. We calculate the energy spectrum of GWs and show that the peak is at frequencies around nanohertz, which is within the frequency range of SKA and EPTA, and lies in the 2σ uncertainty of the NANOGrav constraints. In addition, around millihertz, the curves lie above the expected sensitivity curves of ASTROD-GW, so it can be detected in near future.

After inflation ends, we assume that the inflaton is coupled with SM Higgs boson and singlet fermionic dark matter field. We analyze the reheating temperature, calculate the effect of one-loop CW corrections of the coupling terms, combined with the bounds of BBN, Lyman-α, etc, we constrain the coupling parameters as $y_\chi < 1.00687 \times 10^{-4}$ and $2.7451 \times 10^{-23} < \lambda_{12}/M_p < 3.03996 \times 10^{-8}$. We also discuss the dark matter production of inflaton decay, inflaton scattering and SM scattering, and find that the main way to produce dark matter is the direct decay of inflaton. If we assume that the inflaton decay process produces the whole DM abundance, the parameter y_χ should satisfies $2.081 \times 10^{-27} < y_\chi < 5.294 \times 10^{-6}$.

Acknowledgements This work was supported by "the National Natural Science Foundation of China" (NNSFC) with Grant No. 11705133, and by the "Natural Science Basic Research Program of Shaanxi (Program No. 2023-JC-YB-072)".

Data Availability Statement This manuscript has no associated data or the data will not be deposited. [Authors' comment: This is a theoretical study and the results can be obtained explicitly from the relevant calculations presented in this paper.]

Funded by SCOAP[3]. SCOAP[3] supports the goals of the International Year of Basic Sciences for Sustainable Development.

References

1. Z. Arzoumanian et al. [NANOGrav], Astrophys. J. Lett. **905**(2), L34 (2020). arXiv:2009.04496 [astro-ph.HE]
2. V. Vaskonen, H. Veermäe, Phys. Rev. Lett. **126**(5), 051303 (2021). arXiv:2009.07832 [astro-ph.CO]
3. K. Kohri, T. Terada, Phys. Lett. B **813**, 136040 (2021). arXiv:2009.11853 [astro-ph.CO]
4. V. De Luca, G. Franciolini, A. Riotto, Phys. Rev. Lett. **126**(4), 041303 (2021). arXiv:2009.08268 [astro-ph.CO]
5. M. Kawasaki, H. Nakatsuka, arXiv:2101.11244 [astro-ph.CO]
6. S. Vagnozzi, Mon. Not. R. Astron. Soc. **502**(1), L11–L15 (2021). arXiv:2009.13432 [astro-ph.CO]
7. G. Domènech, S. Pi, arXiv:2010.03976 [astro-ph.CO]
8. S. Matarrese, S. Mollerach, M. Bruni, Phys. Rev. D **58**, 043504 (1998). arXiv:astro-ph/9707278
9. V. Acquaviva, N. Bartolo, S. Matarrese, A. Riotto, Nucl. Phys. B **667**, 119 (2003). arXiv:astro-ph/0209156
10. H. Assadullahi, D. Wands, Phys. Rev. D **79**, 083511 (2009). arXiv:0901.0989 [astro-ph.CO]
11. L. Alabidi, K. Kohri, M. Sasaki, Y. Sendouda, JCAP **1209**, 017 (2012). arXiv:1203.4663 [astro-ph.CO]
12. L. Alabidi, K. Kohri, M. Sasaki, Y. Sendouda, JCAP **1305**, 033 (2013). arXiv:1303.4519 [astro-ph.CO]
13. K. Kohri, T. Terada, Phys. Rev. D **97**(12), 123532 (2018). arXiv:1804.08577 [gr-qc]
14. R.G. Cai, S. Pi, M. Sasaki, Phys. Rev. Lett. **122**(20), 201101 (2019). arXiv:1810.11000 [astro-ph.CO]
15. K. Inomata, T. Nakama, Phys. Rev. D **99**(4), 043511 (2019). arXiv:1812.00674 [astro-ph.CO]
16. R.G. Cai, S. Pi, S.J. Wang, X.Y. Yang, arXiv:1901.10152 [astro-ph.CO]
17. J. Fumagalli, S. Renaux-Petel, L.T. Witkowski, arXiv:2012.02761 [astro-ph.CO]
18. J. Garcia-Bellido, M. Peloso, C. Unal, JCAP **09**, 013 (2017). arXiv:1707.02441 [astro-ph.CO]
19. C. Unal, Phys. Rev. D **99**(4), 041301 (2019). arXiv:1811.09151 [astro-ph.CO]
20. G. Domènech, Int. J. Mod. Phys. D **29**(03), 2050028 (2020). arXiv:1912.05583 [gr-qc]
21. G. Domènech, M. Sasaki, Phys. Rev. D **103**(6), 063531 (2021). arXiv:2012.14016 [gr-qc]
22. G. Domènech, arXiv:2109.01398 [gr-qc]
23. J. Garcia-Bellido, E.R. Morales, Phys. Dark Univ. **18**, 47 (2017). arXiv:1702.03901 [astro-ph.CO]
24. C. Germani, T. Prokopec, Phys. Dark Univ. **18**, 6–10 (2017). arXiv:1706.04226 [astro-ph.CO]
25. H. Di, Y. Gong, JCAP **1807**(07), 007 (2018). arXiv:1707.09578 [astro-ph.CO]
26. G. Ballesteros, M. Taoso, Phys. Rev. D **97**(2), 023501 (2018). arXiv:1709.05565
27. I. Dalianis, A. Kehagias, G. Tringas, JCAP **1901**, 037 (2019). arXiv:1805.09483 [astro-ph.CO]
28. T.J. Gao, X.Y. Yang, Int. J. Mod. Phys. A **34**(32), 1950213 (2019)
29. J.M. Ezquiaga, J. Garcia-Bellido, E.R. Morales, Phys. Lett. B **776**, 345–349 (2018). arXiv:1705.04861 [astro-ph.CO]
30. F. Bezrukov, M. Pauly, J. Rubio, JCAP **02**, 040 (2018). arXiv:1706.05007 [hep-ph]
31. M. Drees, Y. Xu, arXiv:1905.13581 [hep-ph]

32. O. Özsoy, S. Parameswaran, G. Tasinato, I. Zavala, JCAP **07**, 005 (2018). arXiv:1803.07626 [hep-th]
33. T.J. Gao, X.Y. Yang, Int. J. Mod. Phys. A **34**(32), 1950213 (2019)
34. M. Cicoli, V.A. Diaz, F.G. Pedro, JCAP **06**, 034 (2018). https://doi.org/10.1088/1475-7516/2018/06/034. arXiv:1803.02837 [hep-th]
35. J. Liu, Z.K. Guo, R.G. Cai, Phys. Rev. D **101**(8), 083535 (2020). arXiv:2003.02075 [astro-ph.CO]
36. Y. Akrami et al. [Planck Collaboration], arXiv:1807.06211 [astro-ph.CO]
37. S.R. Coleman, E.J. Weinberg, Radiative corrections as the origin of spontaneous symmetry breaking. Phys. Rev. D **7**, 1888 (1973)
38. E.J. Weinberg, arXiv:hep-th/0507214
39. S. Sarkar, Big bang nucleosynthesis and physics beyond the standard model. Rep. Prog. Phys. **59**, 1493 (1996). arXiv:hep-ph/9602260
40. M. Kawasaki, K. Kohri, N. Sugiyama, MeV scale reheating temperature and thermalization of neutrino background. Phys. Rev. D **62**, 023506 (2000). arXiv:astro-ph/0002127
41. S. Hannestad, What is the lowest possible reheating temperature? Phys. Rev. D **70**, 043506 (2004). arXiv:astro-ph/0403291
42. F. De Bernardis, L. Pagano, A. Melchiorri, New constraints on the reheating temperature of the universe after WMAP-5. Astropart. Phys. **30**, 192 (2008)
43. P.F. de Salas, M. Lattanzi, G. Mangano, G. Miele, S. Pastor, O. Pisanti, Bounds on very low reheating scenarios after Planck. Phys. Rev. D **92**, 123534 (2015). arXiv:1511.00672
44. I. Masina, Dark matter and dark radiation from evaporating primordial black holes. Eur. Phys. J. Plus **135**, 552 (2020). arXiv:2004.04740
45. V. Iršič et al., New constraints on the free-streaming of warm dark matter from intermediate and small scale Lyman-α forest data. Phys. Rev. D **96**, 023522 (2017). arXiv:1702.01764
46. N. Bhaumik, R.K. Jain, JCAP **01**, 037 (2020). arXiv:1907.04125 [astro-ph.CO]
47. K. Enqvist, A. Mazumdar, Phys. Rep. **380**, 99–234 (2003). arXiv:hep-ph/0209244
48. C.P. Burgess, H.M. Lee, M. Trott, JHEP **09**, 103 (2009). arXiv:0902.4465 [hep-ph]
49. F. Marchesano, G. Shiu, A.M. Uranga, JHEP **09**, 184 (2014). arXiv:1404.3040 [hep-th]
50. M.P. Hertzberg, M. Yamada, Phys. Rev. D **97**, 083509 (2018). arXiv:1712.09750 [astro-ph.CO]
51. G. Ballesteros, J. Rey, M. Taoso, A. Urbano, JCAP **07**, 025 (2020). arXiv:2001.08220 [astro-ph.CO]
52. C. Germani, T. Prokopec, Phys. Dark Univ. **18**, 6 (2017). arXiv:1706.04226 [astro-ph.CO]
53. K. Dimopoulos, Phys. Lett. B **775**, 262 (2017). arXiv:1707.05644 [hep-ph]
54. J.M. Ezquiaga, J. García-Bellido, JCAP **1808**, 018 (2018). arXiv:1805.06731 [astro-ph]
55. D. Cruces, C. Germani, T. Prokopec, JCAP **1903**(03), 048 (2019). arXiv:1807.09057 [gr-qc]
56. D.J. Schwarz, C.A. Terrero-Escalante, A.A. Garcia, Phys. Lett. B **517**, 243 (2001). arXiv:astro-ph/0106020
57. S.M. Leach, A.R. Liddle, J. Martin, D.J. Schwarz, Phys. Rev. D **66**, 023515 (2002). arXiv:astro-ph/0202094
58. D.J. Schwarz, C.A. Terrero-Escalante, JCAP **0408**, 003 (2004). arXiv:hep-ph/0403129
59. T.S. Bunch, P.C.W. Davies, Proc. R. Soc. Lond. A **360**, 117–134 (1978)
60. C.T. Byrnes, P.S. Cole, S.P. Patil, JCAP **06**, 028 (2019). arXiv:1811.11158 [astro-ph.CO]
61. D. Baumann, P.J. Steinhardt, K. Takahashi, K. Ichiki, Phys. Rev. D **76**, 084019 (2007). arXiv:hep-th/0703290
62. K.N. Ananda, C. Clarkson, D. Wands, Phys. Rev. D **75**, 123518 (2007). arXiv:gr-qc/0612013
63. K. Ando, K. Inomata, M. Kawasaki, K. Mukaida, T.T. Yanagida, Phys. Rev. D **97**(12), 123512 (2018). arXiv:1711.08956 [astro-ph.CO]
64. H. Kodama, M. Sasaki, Prog. Theor. Phys. Suppl. **78**, 1 (1984)
65. V.F. Mukhanov, H.A. Feldman, R.H. Brandenberger, Phys. Rep. **215**, 203 (1992)
66. J.R. Espinosa, D. Racco, A. Riotto, JCAP **09**, 012 (2018). arXiv:1804.07732 [hep-ph]
67. H. Audley et al., arXiv:1702.00786 [astro-ph.IM]
68. Z.K. Guo, R.G. Cai, Y.Z. Zhang, arXiv:1807.09495 [gr-qc]
69. C.J. Moore, R.H. Cole, C.P.L. Berry, Class. Quantum Gravity **32**(1), 015014 (2015). arXiv:1408.0740 [gr-qc]
70. J. Luo et al. [TianQin Collaboration], Class. Quantum Gravity **33**(3), 035010 (2016). arXiv:1512.02076 [astro-ph.IM]
71. K. Kuroda, W.T. Ni, W.P. Pan, Int. J. Mod. Phys. D **24**(14), 1530031 (2015). arXiv:1511.00231 [gr-qc]
72. M. Drees, Y. Xu, JCAP **09**, 012 (2021). arXiv:2104.03977 [hep-ph]
73. N. Bernal, Y. Xu, Eur. Phys. J. C **81**(10), 877 (2021). arXiv:2106.03950 [hep-ph]
74. A. Ghoshal, G. Lambiase, S. Pal, A. Paul, S. Porey, JHEP **09**, 231 (2022). https://doi.org/10.1007/JHEP09(2022)231. arXiv:2206.10648 [hep-ph]
75. D.J.H. Chung, E.W. Kolb, A. Riotto, Production of massive particles during reheating. Phys. Rev. D **60**, 063504 (1999). arXiv:hep-ph/9809453
76. G.F. Giudice, E.W. Kolb, A. Riotto, Largest temperature of the radiation era and its cosmological implications. Phys. Rev. D **64**, 023508 (2001). arXiv:hep-ph/0005123
77. N. Bernal, F. Elahi, C. Maldonado, J. Unwin, Ultraviolet freeze-in and non-standard cosmologies. JCAP **11**, 026 (2019). arXiv:1909.07992 [hep-ph]
78. M. Drees, F. Hajkarim, E.R. Schmitz, The effects of QCD equation of state on the relic density of WIMP dark matter. JCAP **06**, 025 (2015). arXiv:1503.03513
79. Y. Mambrini, K.A. Olive, Gravitational production of dark matter during reheating. arXiv:2102.06214
80. N. Bernal, C.S. Fong, Dark matter and leptogenesis from gravitational production. arXiv:2103.06896
81. B. Barman, N. Bernal, Gravitational SIMPs. arXiv:2104.10699
82. M. Garny, M. Sandora, M.S. Sloth, Planckian interacting massive particles as dark matter. Phys. Rev. Lett. **116**, 101302 (2016). arXiv:1511.03278
83. Y. Tang, Y.-L. Wu, On thermal gravitational contribution to particle production and dark matter. Phys. Lett. B **774**, 676 (2017). arXiv:1708.05138
84. N. Bernal, M. Dutra, Y. Mambrini, K. Olive, M. Peloso, M. Pierre, Spin-2 portal dark matter. Phys. Rev. D **97**, 115020 (2018). arXiv:1803.01866
85. J. Yokoyama, Astron. Astrophys. **318**, 673 (1997). arXiv:astro-ph/9509027
86. J. Garcia-Bellido, A.D. Linde, D. Wands, Phys. Rev. D **54**, 6040 (1996). arXiv:astro-ph/9605094
87. S. Clesse, J. Garcia-Bellido, Phys. Rev. D **92**(2), 023524 (2015). arXiv:1501.07565 [astro-ph.CO]
88. J. Garcia-Bellido, M. Peloso, C. Unal, JCAP **1612**(12), 031 (2016). arXiv:1610.03763 [astro-ph.CO]
89. S.L. Cheng, W. Lee, K.W. Ng, JHEP **1702**, 008 (2017). arXiv:1606.00206 [astro-ph.CO]
90. C. Fu, P. Wu, H. Yu, arXiv:1907.05042 [astro-ph.CO]